HHS Public Access

Author manuscript

Opt Lett. Author manuscript; available in PMC 2018 March 29.

Published in final edited form as:

Opt Lett. 2014 January 15; 39(2): 186–188.

Compact piezoelectric transducer fiber scanning probe for optical coherence tomography

Ning Zhang[1,2], **Tsung-Han Tsai**[1], **Osman O. Ahsen**[1], **Kaicheng Liang**[1], **Hsiang-Chieh Lee**[1], **Ping Xue**[2], **Xingde Li**[3], and **James G. Fujimoto**[1,*]

[1]Department of Electrical Engineering and Computer Science and Research Laboratory of Electronics, Massachusetts Institute of Technology, Cambridge, Massachusetts 02139, USA

[2]State Key Laboratory of Low-Dimensional Quantum Physics and Laboratory of Atomic and Molecular Nanosciences Department of Physics, Tsinghua University, Beijing 100084, China

[3]Department of Biomedical Engineering, Johns Hopkins University, Baltimore, Maryland 21205, USA

Abstract

We developed a compact, optical fiber scanning piezoelectric transducer (PZT) probe for endoscopic and minimally invasive optical coherence tomography (OCT). Compared with previous forward-mount fiber designs, we present a reverse-mount design that achieves a shorter rigid length. The fiber was mounted at the proximal end of a quadruple PZT tube and scanned inside the hollow PZT tube to reduce the probe length. The fiber resonant frequency was 338 Hz using a 17-mm-long fiber. A 0.9 mm fiber deflection was achieved with a driving amplitude of 35 V. Using a GRIN lens-based optical design with a 1.3× magnification, a ~6 μm spot was scanned over a 1.2 mm diameter field. The probe was encased in a metal hypodermic tube with a ~25 mm rigid length and covered with a 3.2 mm outer diameter (OD) plastic sheath. Imaging was performed with a swept source OCT system based on a Fourier domain modelocked laser (FDML) light source at a 240 kHz axial scan rate and 8 μm axial resolution (in air). *En face* OCT imaging of skin *in vivo* and human colon *ex vivo* was demonstrated.

Optical coherence tomography (OCT) performs cross-sectional, micrometer-resolution imaging of tissue pathology [1]. The development of fiber-optic OCT endoscopic probes enabled imaging of internal organs [2,3]. Multiple endoscopic OCT probe designs have been demonstrated for internal body imaging [2–9]. There are two general categories of probes: side imaging and forward imaging. Most side-imaging probes proximally rotate an optical assembly using a torque cable [3] or distally actuate a mirror [4] to generate a rotary scan perpendicular to the axis of the probe. Three-dimensional (3D) data can be acquired using proximal pullback of the optical assembly to scan a helical pattern. However, probe designs with proximal actuations have scanning instabilities, making it challenging to obtain a good quality 3D or *en face* imaging, especially in endoscopic applications that require long probe length.

*Corresponding author: jgfuji@mit.edu.

Forward-imaging probes have the advantage that they can be easily positioned over tissue regions of interest [7,8]. More importantly, they enable precise two-dimensional (2D) forward-scanning imaging and are well suited for 3D OCT or optical coherence microscopy. There are several forward-imaging probe designs, such as deformable polymers [10], microelectromechanical system scanners [11], and piezolever fiber scanners [12].

For endoscopic OCT, it is important to image a wide field of view with a small-probe outer diameter (OD) and short rigid length, so that the probe can be inserted into a 2.8 mm or 3.7 mm endoscope accessory port. The quadruple piezoelectric transducer (PZT) actuator is attractive because of its small size and high transverse scanning speed [13]. By driving the PZT with two modulated sinusoidal waves in quadrature at the fiber resonant frequency, a 2D spiral scan pattern can be generated. The transverse scanning speed of the probe is determined by the fiber resonant frequency, which is inversely proportional to the square of the fiber length. The ratio of the fiber transverse deflection range to its mode-field diameter determines the number of resolvable spots. In order to achieve a sufficient fiber deflection range (0.5–1 mm) using PZT drive voltages within electrical safety limits (IEC 60601-1, 3rd edition), the fiber length is typically 15–30 mm [7,8,13,14]. Given the length of the PZT, optics and fiber, the probe rigid length can be as long as 30–40 mm by using a conventional forward-mount design where the fiber is fixed at the distal end of the PZT. Probes with rigid length >20–25 mm are difficult to introduce into the endoscope accessory port, even with small ODs.

This Letter presents a PZT probe design using a reverse-mount fiber to reduce the rigid length, while maintaining a similar scanning performance as conventional forward-mount designs. In the reverse-mount design, the scanning fiber is actuated from the proximal end of the quadruple PZT and scans inside the PZT tube. This design enables more freedom of design parameters, such as fiber and PZT length, and optical magnification, given the device size constraints.

A schematic diagram of the reverse-mount PZT probe is shown in Figs. 1(a) and 1(b). The probe consisted of a quadruple PZT, a pinhole, scanning fiber, and objective lens. The outer electrode surface of the PZT tube was divided into four quadrants, thus forming two pairs of electrodes ($\pm x$, $\pm y$). The PZT tube was lead zirconate titanate with 1.5 mm OD, 0.3 mm wall thickness, and 12.7 mm length. A nonconductive mount was fixed to the distal end and a 500 μm pinhole was used to actuate the fiber at the proximal end. Two hypotubes were used for centering the pinhole and PZT. A 460 μm OD hypotube was inserted into the pinhole, while a larger 0.6 mm inner diameter (ID) and 0.8 mm OD hypotube was inserted into the PZT. The small tube was inserted into the larger tube and the pinhole and PZT were attached with UV epoxy. The proximal fiber was fixed in a hypotube, which covered the entire end. The pinhole design not only confines the epoxy, but also allows the fiber to flex at the attachment point thus enabling more effective actuation. If the fiber was fixed with the proximal end of the PZT without the pinhole design, the fiber deflection would measure ~470 μm, which is ~50% of the deflection of the standard forward-mount design with the same driving voltage. When the fiber is forward mounted, the PZT tube angle and displacement actuation occur in the same direction, thus producing an additive effect. However, when the fiber is reverse mounted and attached to the proximal end of the PZT, the angle actuates in the opposite

direction from the displacement. Therefore, the fiber should be mounted such that the PZT tube displacement is transmitted to the fiber, while the angle is free to vary. This produces a lever action that scales the fiber scan range as the ratio of the total fiber length to lever arm length, as shown in Figs. 1(a) and 1(b). A 17-mm-long, single-mode SMF-28 fiber was attached to the PZT at 1 mm from the fiber proximal end. The fiber was inside the PZT tube with <5 mm protruding. A GRIN lens with a 0.29 pitch and 1.8 mm OD was used as the objective to image the scanned fiber onto the tissue. The fiber was 1 mm from the GRIN lens, thus providing a ~1.3× magnification with a ~2 mm working distance and an estimated ~6 μm focused spot (ω, $1/e^2$ radius) with a 180 μm confocal parameter. The spot size is consistent with the fiber mode field diameter (9.2 ± 0.4 μm) and magnification. The spot size can be adjusted by the fiber to GRIN lens distance. The fiber was angle-cleaved at 8° to reduce the backreflection to < − 50 dB.

By applying triangular-modulated, 90° phase-shifted sinusoidal driving signals to the orthogonal electrode-pairs of PZT at the fiber resonant frequency, the probe generated a spiral scanning pattern that covers a circular field of view [7]. The transverse deflection range of the fiber tip was ~0.9 mm (±0.45 mm) when the PZT was driven with a 35 V amplitude at a resonant frequency of 338 Hz. The transverse field of view was 1.2 mm, which was determined by the fiber deflection range multiplied by the objective magnification. The hypotube cover had a 2.4 mm OD and 2.15 mm ID with a ~25 mm rigid length. The total length including the fiber and wires was 2.17 m. The entire probe was encased in a waterproof plastic tube with 3.2 mm OD covering the hypotube, fiber, and wires. Figure 1(c) is a photo of the probe. The reverse-mount design reduces the rigid length by >30% when compared to an equivalent forward-mount design, which had a ~37 mm rigid length.

The fiber length between the mount at the proximal end and PZT actuation point (lever arm length) is an important parameter for optimizing fiber scanning. Figure 2(a) shows the fiber transverse deflection for different lever arm lengths. There is an optimal length to achieve maximum fiber deflection due to optimized lever action and mechanical impedance matching, as discussed in Ref. [15]. For this design, the maximum deflection was with a ~1 mm lever arm length.

To evaluate the performance of the different PZT probe designs, we compared the reverse-mount with the forward-mount design by using identical PZT and fiber lengths. The fiber deflection range of both designs increased linearly with PZT drive voltage. The deflection transfer function was 12.4 μm/V for reverse-mount and 14.4 μm/V for forward-mount designs. The frequency response was also measured, as shown in Fig. 2(b). The resonant frequencies were 338 and 330 Hz in reverse- and forward-mount designs, respectively. The small frequency difference was caused by a ~1% difference in the fiber lengths. The 3 dB frequency bandwidths were ~6 Hz and ~5.5 Hz for the reverse- and forward-mount designs, which corresponds to quality factors (Qs) of 56.3 and 60, and defines the ratio of the resonance frequency to resonance bandwidth [13]. The deflection range of the reverse-mount design was slightly less than the forward-mount design, possibly because the pinhole impedes angular motion or decreases the Q. In addition, the reverse-mount design is more

complex to fabricate and requires setting an exact lever arm length. However, the reverse design is significantly shorter than the forward design and achieves similar deflection.

To test the imaging performance of the reverse-mount probe, we used a swept source OCT (SS-OCT) system with a double-buffered FDML laser operating at a 240 kHz axial scan rate with a 95 nm FWHM sweep bandwidth centered at 1315 nm, thus yielding an ~8 μm axial resolution (in air). The OCT interferometer used a dual-circulator configuration and dual-balanced detectors with ~200 MHz bandwidth. A Mach–Zehnder interferometer (MZI) was used to calibrate the OCT signal from equal time to equal frequency sampling. The MZI and OCT signals were digitized by a 500 MSPS, 12-bit A/D card (Alazar), which was triggered by the FDML laser. The imaging depth (−6 dB, in air) range was ~2.5 mm. The experimentally measured sensitivity was ~95 dB at an incident power of 18 mW. The sensitivity was lower than the theoretical limit because of increased noise from parasitic backreflections from the GRIN lens surfaces. Dispersion mismatch between the two arms was numerically compensated. The triangular signal modulation period was 2 s, thus corresponding to 1 frame per second with 338 cycles per frame and 710 A-lines per cycle. Remapping the axial scan spiral positions to Cartesian coordinates was required to generate volumetric data and visualization of *en face* images. Figure 3(a) shows a microscope photo of a test grid pattern with ~250 μm spacing and ~70 μm linewidth, and Fig. 3(b) shows the reconstructed *en face* OCT image of the grid. In Fig. 3, a gray-scale OCT display is used instead of inverse gray scale to facilitate comparison with the photo. These results demonstrate a good reconstruction of the *en face* OCT images from spiral scanning pattern with minimal distortion. Figure 3(c) shows a measurement of the transverse resolution by imaging an USAF 1951 resolution chart with a reduced fiber scanning range. The elements with a 6.2 μm width can be clearly visualized. The image has weak signals on the periphery because the OCT beam angle varies during scanning and the target is flat and reflective.

The performance of the reverse-mount probe was investigated by imaging human skin *in vivo* and human colon specimens *ex vivo*. Figure 4(a) shows OCT images of a human fingertip with a representative cross-sectional image. The stratum corneum, stratum spinosum, and a sweat duct can be visualized. Figure 4(b) shows *en face* images at different depths (from 120 to 300 μm, 60 μm apart). The ridge structures and dark dots, indicated by arrows, are fingerprint ridges and sweat ducts, respectively. Figure 5(a) shows an *en face* OCT image of a freshly excised human colon specimen. The study protocol was approved by the MIT COUHES and BIDMC IRB committees, and discarded specimens not required for clinical diagnosis were used. Round crypt structures, indicated by arrows, are seen with mucous containing crypt lumens exhibiting high contrast relative to the surrounding epithelium, visible as a dark ring. The lamina propria surrounding the crypts can also be identified.

In conclusion, we demonstrated a compact reverse-mount fiber scanning PZT probe that reduces rigid length while maintaining comparable performance to forward-mount probes. The probe had a ~25 mm rigid length with a 2.4 mm OD hypotube and a 3.2 mm OD plastic sheath. *En face* OCT imaging with high 2D scanning stability was demonstrated with an SS-OCT system using an FDML light source.

Acknowledgments

We thank Drs. Y. Sheikine and J. Connolly from the Beth Israel Deaconess Medical Center for providing *ex vivo* human specimens. The research was sponsored in part by the National Institutes of Health (R01-CA75289-17, R44-CA101067-06, R01-EY011289-27, R01-HL095717-04, and R01-NS057476-05), Air Force Office of Scientific Research (FA9550-12-1-0499), and Medical Free Electron Laser Program (FA9550-10-1-0551). N. Zhang was partially supported by the China Scholarship Council.

References

1. Huang D, Swanson EA, Lin CP, Schuman JS, Stinson WG, Chang W, Hee MR, Flotte T, Gregory K, Puliafito CA, Fujimoto JG. Science. 1991; 254:1178. [PubMed: 1957169]
2. Tearney GJ, Brezinski ME, Bouma BE, Boppart SA, Pitris C, Southern JF, Fujimoto JG. Science. 1997; 276:2037. [PubMed: 9197265]
3. Adler DC, Chen Y, Huber R, Schmitt J, Connolly J, Fujimoto JG. Nat. Photonics. 2007; 1:709.
4. Herz PR, Chen Y, Aguirre AD, Schneider K, Hsiung P, Fujimoto JG, Madden K, Schmitt J, Goodnow J, Petersen C. Opt. Lett. 2004; 29:2261. [PubMed: 15524374]
5. Suter MJ, Vakoc BJ, Yachimski PS, Shishkov M, Lauwers GY, Mino-Kenudson M, Bouma BE, Nishioka NS, Tearney GJ. Gastroint. Endosc. 2008; 68:745.
6. Seibel EJ, Smithwick QYJ. Lasers Surg. Med. 2002; 30:177. [PubMed: 11891736]
7. Liu XM, Cobb MJ, Chen YC, Kimmey MB, Li XD. Opt. Lett. 2004; 29:1763. [PubMed: 15352362]
8. Huo L, Xi JF, Wu YC, Li XD. Opt. Express. 2010; 18:14375. [PubMed: 20639922]
9. Tsai T, Potsaid B, Kraus MF, Zhou C, Tao YK, Hornegger J, Fujimoto JG. Biomed. Opt. Express. 2011; 2:2438. [PubMed: 21833379]
10. Wang YL, Bachman M, Li GP, Guo SG, Wong BJF, Chen ZP. Opt. Lett. 2005; 30:53. [PubMed: 15648635]
11. Park HC, Song C, Kang M, Jeong Y, Jeong KH. Opt. Lett. 2012; 37:2673. [PubMed: 22743491]
12. Aguirre AD, Sawinski J, Huang SW, Zhou C, Denk W, Fujimoto JG. Opt. Express. 2010; 18:4222. [PubMed: 20389435]
13. Moon S, Lee S-W, Rubinstein M, Wong BJF, Chen Z. Opt. Express. 2010; 18:21183. [PubMed: 20941015]
14. Xi JF, Chen YP, Zhang YY, Murari K, Li MJ, Li XD. Opt. Lett. 2012; 37:362. [PubMed: 22297353]
15. Sawinski, J. Ph.D. dissertation. Ruperto-Carola University of Heidelberg; 2005. Development of a head-mount fiber scanning system for imaging in vivo.

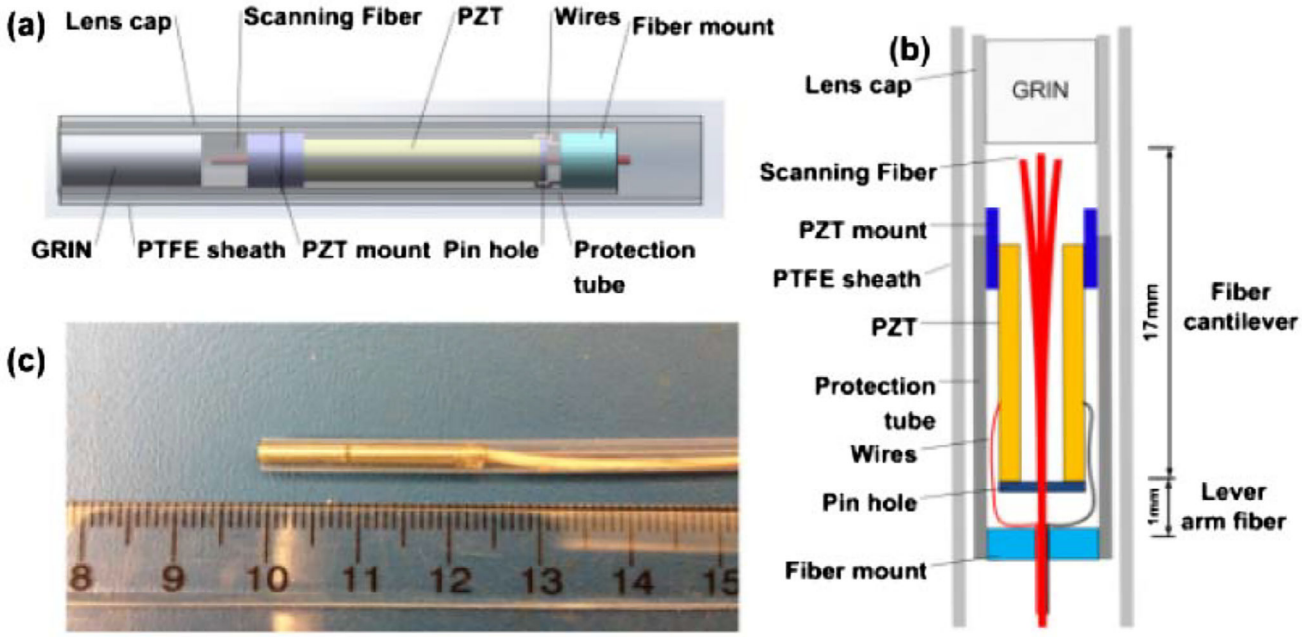

Fig. 1.

(a) Schematic, (b) cross-sectional view, and (c) photo of reverse-mount probe.

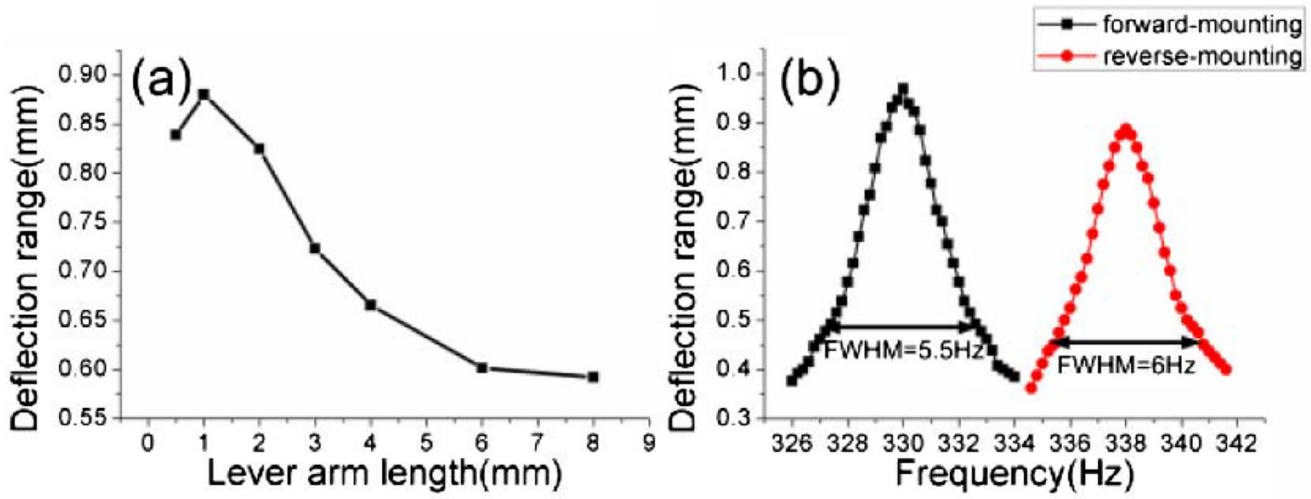

Fig. 2.

(a) Fiber deflection range versus lever arm length. (b) The frequency response of reverse-mount and forward-mount probes.

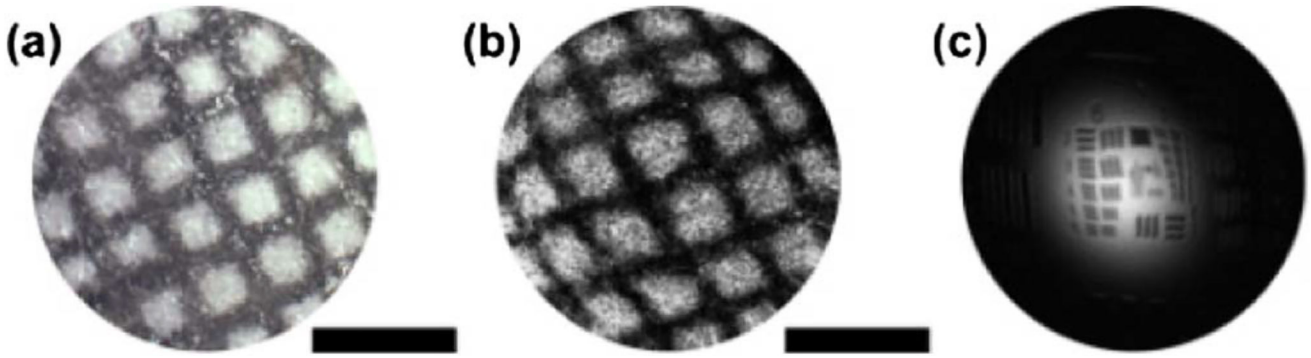

Fig. 3.

(a) Microscope photo of test grid pattern. (b) *En face* OCT image of the test grid pattern. (c) *En face* OCT image of a USAF resolution chart. The scale bars are 500 μm.

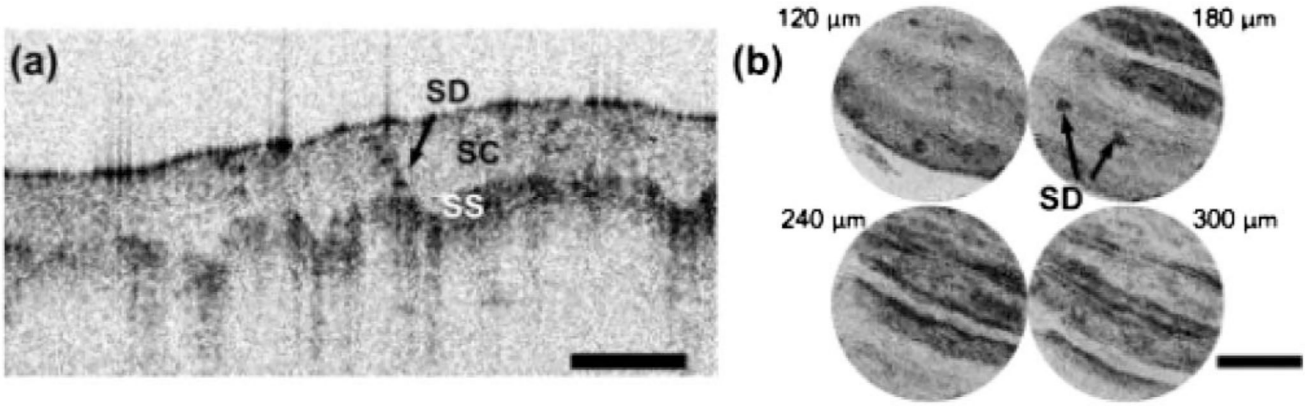

Fig. 4.

(a) OCT image of human finger. (b) *En face* images at depths of 120–300 μm, 60 μm apart. SC, stratum corneum; SS, stratum spinosum; SD, sweat duct. Scale bars 500 μm.

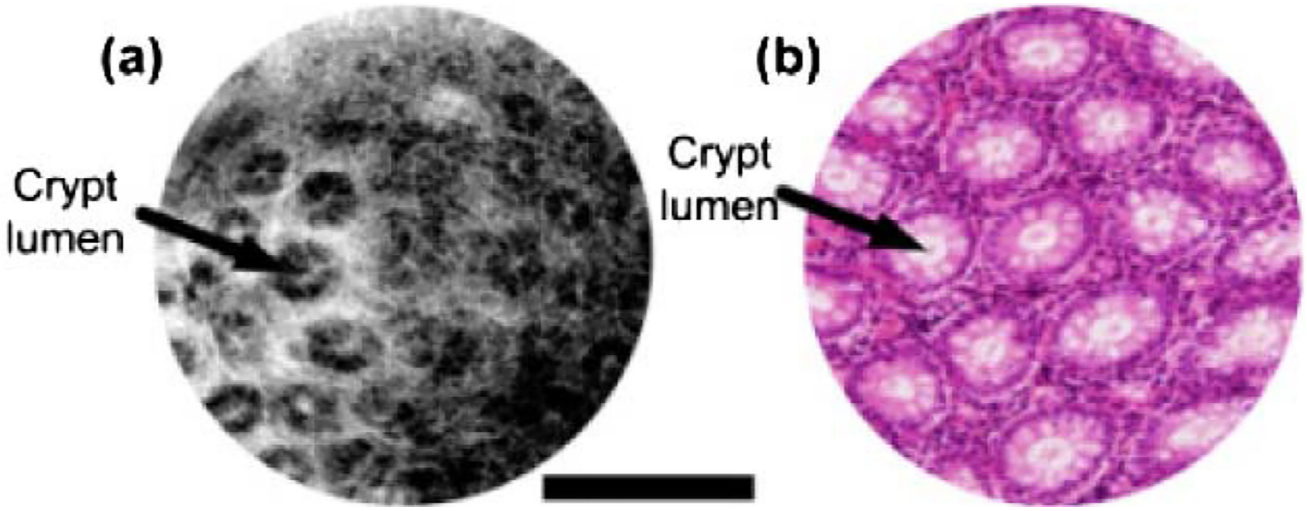

Fig. 5.

Freshly excised human colon. (a) *En face* OCT image at ~90 μm depth. (b) Representative histology with hematoxylin and eosin (H&E) stain. Scale bar 500 μm